RESEARCH

Thermal stratification affects comfort and air quality in naturally ventilated amphitheater classrooms

P. G. Ledda[1] · M. G. Badas[1] · P. Monti[2] · A. Pelliccioni[3] · G. Querzoli[1]

Received: 26 February 2026 / Revised: 1 June 2026 / Accepted: 5 June 2026

Abstract
We numerically investigate the steady mean turbulent flow and temperature fields developing in a model of an amphitheater classroom affected by stratification, and the associated consequences on thermal comfort, and air quality. The classroom is ventilated through external doors, warmed by the occupants and exchanges heat through the walls. The fluid dynamics is governed mainly by the competition between the momentum of the incoming air and buoyancy due to occupants' heat fluxes as well as inflow temperature. The inflow velocity is the primary determinant of the indoor conditions: when low occupants' heat fluxes dominate, the resulting stratification leads to poor air quality and reduced comfort in the upper tiers. Conversely, higher inlet velocity promotes mixing and prevents stratification, thus homogenizing and reducing the Age of Air. Albeit with less intensity, thermal stratification is also observed with low external temperature. Conversely, high external temperatures enhance mixing, improving the overall comfort and air quality. These findings highlight flow structures in a level of detail that complements previous literature and contributes to the understanding of buoyancy-driven ventilation in rooms of large height and complex geometry, such as auditoriums.

Keywords Amphitheater classroom · RANS · Ventilation · Stratification · Thermal comfort · Air quality

1 Introduction

The effectiveness of an indoor environment in ensuring comfort and health of occupants is largely determined by thermal conditions and air quality. Poor indoor air quality is considered a threatening factor for human health [1–4] and involves particulate matter as well as volatile organic compounds [5–7]. The presence of contaminant particles may cause discomfort to the eyes, irritation of the respiratory system, as well as may spread diseases [8].

Indoor air quality has gained increasing interest in the last decades [9, 10]. Forced ventilation, heating and air conditioning systems are responsible for a significant portion (about half) of building energy consumption. Therefore, natural ventilation is an effective and low energy-consuming approach to control these factors whose effectiveness is often measured by the Age of Air (AOA), i.e. the average time that an air parcel takes to travel from an inlet to the assigned point [11]. The Local Mean Age (LMA) is obtained when the concentration decay is assessed locally within the same room. Larger (smaller) values of LMA depict reduced (increased) fresh air delivery [12]. The volume average of local measurements of LMA gives the Mean Age of Air (MAA), an index largely employed for assessing the overall quality of air within an indoor space [13, 14].

Thermal comfort is another crucial aspect for evaluating the adequacy of an indoor environment whose primary function is to host people. According to ASHRAE Standard 55–2004, it can be quantified by two indexes [15]: the

https://doi.org/10.1007/s11012-026-02147-x

Published online: 19 June 2026

Predicted Mean Vote (PMV), based on equations aimed to predict the mean value of the thermal sensation votes expressed by occupants on a scale from -3 (cold) to 3 (hot), and the Predicted Percentage of Dissatisfied (PPD), which quantifies the expected percentage of thermally uncomfortable people, based on PMV [16–19]. The computation of PMV and PPD requires some assumptions about the occupants' metabolic rates and clothing insulation levels for the space being considered. While being a simplified view [20] (compared, e.g., to adaptive comfort approaches [21, 22]) because of the intrinsic ability of people to adapt to thermal variations [23, 24], PMV and PPD can however give useful design information. Human occupation rates and activities influence temperature, humidity, and exhaled air distributions owing to the heat production rate from metabolism, continuous movements acting as a source for airflow motion [25], exhalation [26] and chemical interaction, as well as diffusion from the clothing of a wide variety of particles [27]. Heat sources from occupants and heat exchange of the building with the external environment lead to non-uniform temperature distributions, resulting in the development of buoyant convection [28, 29]. Extensive on-field measurements reported thermal gradients that can easily exceed 1 °C per meter [17]. When unstable thermal conditions are promoted by the indoor heat exchanges, buoyant coherent structures develop. These structures act as heat and mass transport barriers changing indoor thermal comfort and air quality. Natural and mechanical ventilation requires enough strength to break these structures, which is achieved by sustained and targeted ventilation [29]. Conversely, ventilation rates cannot be too high, since high air speed is often associated with draught discomfort [30]. The interplay between buoyancy and advective transport effects is therefore crucial in defining thermal comfort and air quality [29].

The typically intricate geometries and large number of factors in real-life configurations as well as the complexity of the fluid dynamics and heat transfer make CFD models an effective and reliable tool for indoor thermal comfort and air quality analyses [31–34]. A popular approach relies on integrating Reynolds-Averaged Navier Stokes equations (RANS), which allows for the description of the mean flow features by modeling the turbulent fluctuation effect through additional equations related to turbulent quantities [32]. This approach can capture the essential features of the flow with reasonable computational costs, thereby enabling its use in parametric or optimization analyses to effectively improve both thermal comfort and air quality. Furthermore, RANS models well predict particle concentration resulting from long-term exposure, compared to more refined models such as LES [35].

Achieving effective ventilation in classrooms and lecture halls is a critical issue since, on one hand, they heavily rely on thermal comfort and air quality to properly accomplish their function and, on the other hand, they are subject to the presence of several occupants for long times [36, 37]. Thermal stratification is very likely to be observed due to thermal plumes generated by the occupants' metabolism and possibly by other thermal sources [38]. Several CFD studies focused on rooms with simple geometry and flat floor [39], with particular emphasis on scalar transport in the context of airborne infection. Nevertheless, the fluid dynamics of ventilation in amphitheater classrooms has received less attention, so far.

Within this context, understanding how thermal gradients influence the fluid dynamics gains further interest due to the inhomogeneity of the heat sources along the height and their interaction with localized ventilation openings and, possibly, different wall thermal conditions. To this aim, a well-established engineering method are steady RANS numerical simulations, a reasonable model since rooms remain occupied for hours. At the same time, ventilation remains constant for the same amount of time, much larger than the typical time scales of evolution within the room, of the order of minutes. Therefore, transient effects are neglected because of the large time for which main boundary conditions within the room are hardly modified. This steady, simplified view can be employed as a benchmark for more refined analyses building on these findings. We thus analyse the mean turbulent airflow in a typical university amphitheater classroom, crowded by students and with fresh air coming from one of the doors located at the ground floor level on the wall behind the teacher's desk and exiting from a second door, symmetrically opening on the same wall. The classroom configuration is based on the "Giacomini" classroom at Sapienza University of Rome, which was previously investigated within the "Integrated Evaluation of Indoor Particulate Exposure" (VIEPI) project [40]. In the present model, the room is ventilated through two lower doors located on the front wall: one door is prescribed as the inlet and the other as the outlet (Fig. 1). This

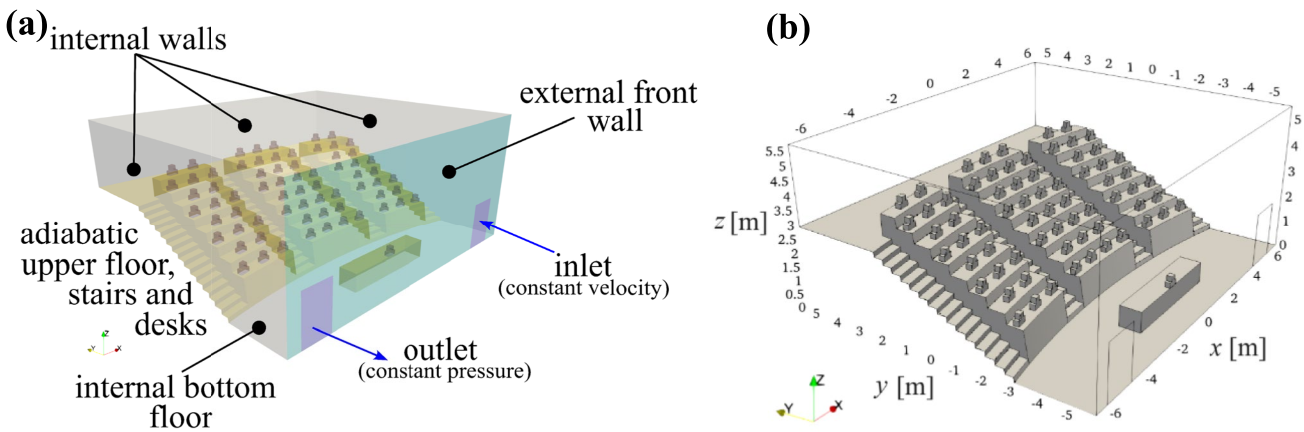

Fig. 1 Sketch of the computational domain with **a** the main boundary conditions and **b** dimensions. Airflow at constant velocity U and fixed external temperature T_e is injected from the inlet. The room internal walls exchange heat with an internal environment set at a constant temperature T_0, while the front wall exchanges heat with the external environment (T_e). Occupants emit a constant heat flux while stairs, desks and upper floor are assumed to be adiabatic

one-inlet/one-outlet arrangement is therefore intended as a realistic reference door-ventilation condition for the considered classroom.

From a theoretical point of view, the objective of the work is to define a systematic fluid-mechanics-based framework to identify and quantify relevant features developing in that complex geometry for different ventilation intensities and external temperatures, as a fundamental building block toward more refined techniques for the flow and boundary conditions description. In addition, from an applicative point of view, we compute integral quantities with the final goal of giving fruitful general information on thermal comfort and air quality in the different zones of the amphitheater classrooms. The paper is structured as follows. Section 2 presents the methods in terms of problem formulation and numerical approach. Section 3 is devoted to the presentation of the velocity and temperature fields developing into the room for different inflow and external temperature conditions, giving practical information on thermal comfort indices. Fluid dynamic fields are then used in Sect. 4, which investigates their implications in terms of Age of Air.

2 Methods: problem formulation and numerical approach

We compute the steady turbulent flow with thermal buoyancy effects in the amphitheater classroom represented in Fig. 1. The classroom dimensions are $L = 13.0$ m, $D = 11.3$ m, and $H = 5.5$ m, along the x, y, and z directions, respectively. The external doors are 1.3 m wide and 2.0 m high. We consider a reference temperature, $T_0 = 20$ °C, in the indoor environment and we denote as $m = 1.5 \cdot 10^{-5}$ Pa s and $r = 1.2$ kg/m^3 the dynamic viscosity and density of the air, respectively. We then indicate with $n = m/r$ the kinematic viscosity. The walls are assumed to exchange heat with the surrounding environment with an exchange coefficient of $h = 1.6$ W/(m^{2}K) (a typical value for brick walls, see e.g. ASHRAE 2001 Handbook [41]). The lateral, bottom ground and ceiling walls are assumed internal and thus they exchange heat with an indoor building environment at temperature T_0 (grey boundaries in Fig. 1), while the front wall (blue in Fig. 1) is considered external and hence exchanges heat with the external temperature T_e. Furthermore, we assume that desks, stairs, and upper ground walls (yellow surfaces in Fig. 1) are adiabatic. The inlet is localized at the right door, with a uniform inlet velocity, U, at the external temperature, T_e. The outlet is located at the left door, where a fixed reference pressure was prescribed while zero gradient conditions were imposed for all other variables (here and in the following we will refer to left and right from the point of view of a person at the desk standing in front of the occupants). This configuration, although simplified, represents a realistic reference door-ventilation configuration of the analyses performed in the VIEPI project [40]. Each occupant emits heat at a constant rate of 62 W/m^2 on a body of typical size of 1.8m^2 [42, 43], typical of people performing an intense sedentary activity [41]. The power emitted by the occupants is divided into a convective (45%) and a radiant fraction (55%), the latter redistributed as a constant heat flux q_r on the room walls, which is added to the conductive heat exchange with the external wall surface [44–47]. The velocity and temperature differences under consideration lead to very large values of the Reynolds number ($Re = \frac{UL}{\nu} \sim 10^6$), thus suggesting the development of a turbulent flow.

The steady flow thus obeys the continuity and Reynolds-Averaged Navier Stokes (RANS) equations that, under the Boussinesq assumption, read:

$$\frac{\partial \overline{u}_j}{\partial x_j} = 0;\ \overline{u}_j \frac{\partial \overline{u}_i}{\partial x_j} = -\frac{1}{\rho_0}\left(\frac{\partial \overline{p}}{\partial x_i}\right) + \frac{\overline{\rho}\left(\overline{T}\right)}{\rho_0} g_i + \nu \frac{\partial^2 \overline{u}_i}{\partial x_j^2} - \overline{u_i^{'} u_j^{'}} \tag{1}$$

where the Einstein notation for repeated indices is adopted.

The variable density in the momentum equations reads $\overline{\rho}\left(\overline{T}\right) = \rho_0 - \rho_0 \beta (\overline{T} - T_0)$, where $\beta = 3.4 \cdot 10^{-3}\ K^{-1}$ is the thermal expansion coefficient. The Reynolds stress tensor is modeled as $-\rho_0 \overline{u_i\prime u_j\prime} = \mu_t \left(\frac{\partial \overline{u}_i}{\partial x_j} + \frac{\partial \overline{u}_j}{\partial x_i}\right) - \frac{2}{3} k \delta_{ij}$, where m_t is the turbulent viscosity, evaluated by the RNG k-ε model, i.e. $\nu_t = f\left(\frac{\rho k^2}{\varepsilon}\right)$, widely recognized to well perform in indoor airflow and buoyancy-driven flows [20, 35, 48–52]. The steady energy equation for the temperature reads:

$$\frac{\partial}{\partial x_j}\left(\overline{T}\overline{u}_j\right) - \frac{\partial}{\partial x_j}\left(\kappa_{\mathrm{eff}} \frac{\partial \overline{T}}{\partial x_j}\right) = 0 \tag{2}$$

where $\kappa_{\mathrm{eff}} = n/Pr + n_t/Pr_t$, $Pr = 0.7$ and $Pr_t = 0.85$, with the latter two indicating the laminar and turbulent Prandtl numbers, respectively [53]. The heat transfer at the walls is modeled by the equation:$k\frac{\partial \overline{T}}{\partial n} + h\left(\overline{T} - T_*\right) = q_r$, where $k = C_p\ \kappa_{\mathrm{eff}}$, $C_p = 1006$ J/(kg K) is the specific heat at constant pressure, n the normal to the wall, and T_* is the assigned temperature (T_0 or T_e, for internal and external wall, respectively). With air and typical values of the parameters employed in this work, the Rayleigh number reaches values of approx.$Ra \sim 10^{11}$, indicating strong natural convection that will compete with the high Reynolds number jet of fresh air from the inlet. The numerical integration is performed within the OpenFOAM® environment [54]. We employ the built-in solver *buoyant-BoussinesqSimpleFoam* while the heat flux boundary conditions are implemented through the utility *groovyBC*. In Appendix A, we report a grid convergence analysis that gives evidence that the results and conclusions exposed in the following sections are independent of the grid size. Additionally, we validated our implementation of the boundary conditions and physical values against an indoor benchmark case, that relies both on numerical and experimental measurements, to ensure the faithfulness of the obtained results in terms of steady, mean, quantities (Appendix B). We note that the characteristic time scale is t = L/ U ~ 100 s, which is orders of magnitude smaller than the time in which the room is occupied without appreciable variations of the boundary conditions (hours), thus justifying the steady state assumption.

Pollutant dispersion and fresh air distribution are studied within the well-assessed steady framework of the Age of Air. Once the steady solution of the flow equations is obtained, mass transport and the subsequent air quality evaluations are modeled via the advection–diffusion equation for local mean age of air q:

$$\frac{\partial}{\partial x_j}\left(\overline{\vartheta}\overline{u}_j\right) - \frac{\partial}{\partial x_j}\left(D \frac{\partial \overline{\vartheta}}{\partial x_j}\right) = 1 \tag{3}$$

where $D = D_0 + \nu_t / Sc_t$, includes both molecular, $D_0 = 2.88 \times 10^{-5}$ m^2/s, and turbulent diffusivity, while Sc_t is the turbulent Schmidt number, assumed equal to 0.7, according to previous studies focused on air quality in indoor environments, see e.g. Abanto et al. [55]. As boundary conditions we impose zero gradient everywhere except at the inlet, where we assign a zero age of air value. From the spatial distribution of the age of air, one can infer the air quality in different zones of the room. The advection–diffusion equation has been implemented by adding the term n_t / Sc_t in the built-in solver *scalarTransportFoam*. To reach the steady state, we use a time-marching procedure with a typical time-step of 0.001 s that ensures a CFL number below 0.1.

3 Results: flow features

The simulations are organized to isolate the effects of inlet momentum and thermal forcing. The reference condition corresponds to $U = 1.0$ m/s and $T_0 = T_e = 20$ °C, representative of a mid-season configuration. Starting from this case, we first vary the inlet velocity while keeping the inlet temperature fixed, considering $U = 0.5$, 1 and 1.25 m/s. We then keep $U = 1.0$ m/s and vary the external temperature, considering a colder ("winter") case, $T_e = 10$ °C, and a warmer ("summer") case, $T_e = 30$ °C. The imposed velocities U = 0.5, 1.0, and 1.25 m/s respectively correspond to inlet volumetric flow rates $Q_{in} = 1.30$, 2.60, and 3.25 m^3/s, respectively. For comparison, using ASHRAE 62.1 [15] values for lecture classrooms/lecture halls with fixed seats, the reference outdoor airflow rate (so-called Breathing Zone Outdoor Airflow) is $Q_{ASHRAE} = R_p\, N + R_a\, A_f$, with $R_p = 3.8$ L s^{-1} person^{-1} and $R_a = 0.3$ L s^{-1} m^{-2}. With N = 69 occupants and $A_f = 146.9$ m^2, $Q_{ASHRAE} = 0.306$ m^3/s. Thus, the imposed inlet flow rates are approximately 4, 8, and 10 times larger than the minimum reference value.

3.1 The reference case: competition between ventilation and stratification

This section presents the main fluid dynamics features observed in the reference case. Figure 2 shows the local temperature deviation compared to the external temperature, $\Delta T = \overline{T} - T_e$, observed with the inlet velocity $U = 1.0$ m/s and "mid-season" outdoor temperature, $T_e = T_0 = 20$ °C. The colormaps at the boundaries indicate higher temperatures at the ceiling. At low heights, one can easily recognize a region of low temperature deviation, aligned with the inlet jet (Fig. 2a). This region expands and deviates toward the center of the room. Increasing the height, the low-temperature region penetrates inside the central and mid-height seats (Fig. 2b).

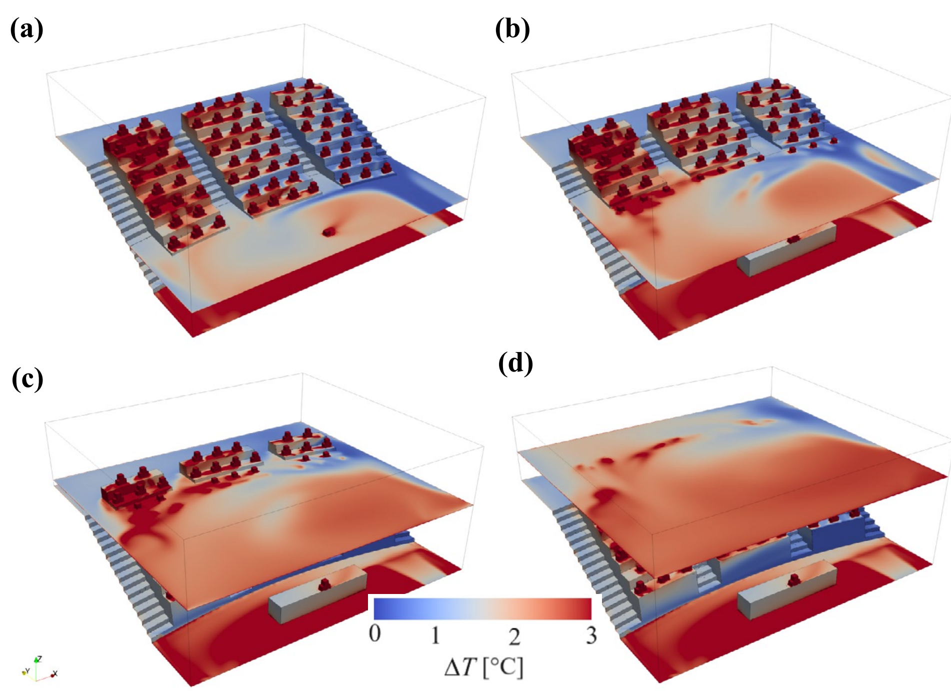

Fig. 2 Colormaps of the temperature deviation compared to the external one $\Delta T = \overline{T} - T_e$, at the walls and over horizontal planes at **a** 1 m, **b** 2 m, **c** 3 m, **d** 4 m height from the ground floor

 https://doi.org/10.1007/s11012-026-02147-x

The inlet jet then reaches and sweeps along the back wall and propagates into the space behind the desks (Figs. 2c and d). Localized spots of relatively high temperature depict the development of thermal plumes, just above some occupants. In general, higher distances from the ground floor are associated with higher temperatures. The highest temperatures are observed in the front of the classroom, above the inlet jet. Hence, for $z \geq 3$ m, the temperature is lower in the rear than in the front part.

Temperature maps suggest that the indoor fluid dynamics is driven by the competition between the thermal plumes rising from the occupants and the jet propagating from the inlet, as shown in Fig. 3. The structure of the fresh-air jet propagating into the room is apparent in Fig. 3a showing the iso-surface at a temperature deviation, $\Delta T = 1$ °C. The incoming flow exhibits a bifurcation, with one branch remaining near the ground floor, ahead of the sloping tiers, and the other branch moving upwards along the stairs between the desks and the right wall, reaching the upper part of the classroom, and eventually descending in the left part of the room. The first branch is characterized by consistently high air speeds, while the upper branch, although remaining coherent for a long path, exhibits speeds approximately halved compared to the first.

Figure 3b shows a set of streamlines originating from the inlet door and confirms the scenario with two recirculating vortices. The first, small but highly coherent, is located on the right side of the inlet door and contributes to redirecting the above-mentioned upper jet branch. The second recirculation is a large zone above the teacher's desk that spans over the whole room height. At the center of the room, the flow is aligned with the tiers and flows toward the left wall. On the left, a stream toward the outlet is observed.

To highlight the competition between the convective plumes generated by the heat flux from the occupants and the advection generated by the inflow, Fig. 3c shows selected positive iso-surfaces of the Q-criterion, colored with the temperature deviation, ΔT. The plot allows one to detect the most relevant small-scale vortical structures in the flow and their buoyancy- or momentum- driven nature. Close to the inlet, vortical structures aligned with the jet break into several elongated cores spreading along the center and rear part of the room. In the space behind the desks, close to the right wall, one can recognize the core of the vortex at low ΔT, due to the roll-up of the inlet flow. However, as the vortical structures propagate towards the center of the room, their temperature increases and, at the same time, they progressively bend upwards. In the left part of the room, the coherent structures are mostly vertical and present the highest temperature difference, indicating that in this region the flow is dominated by thermal convection.

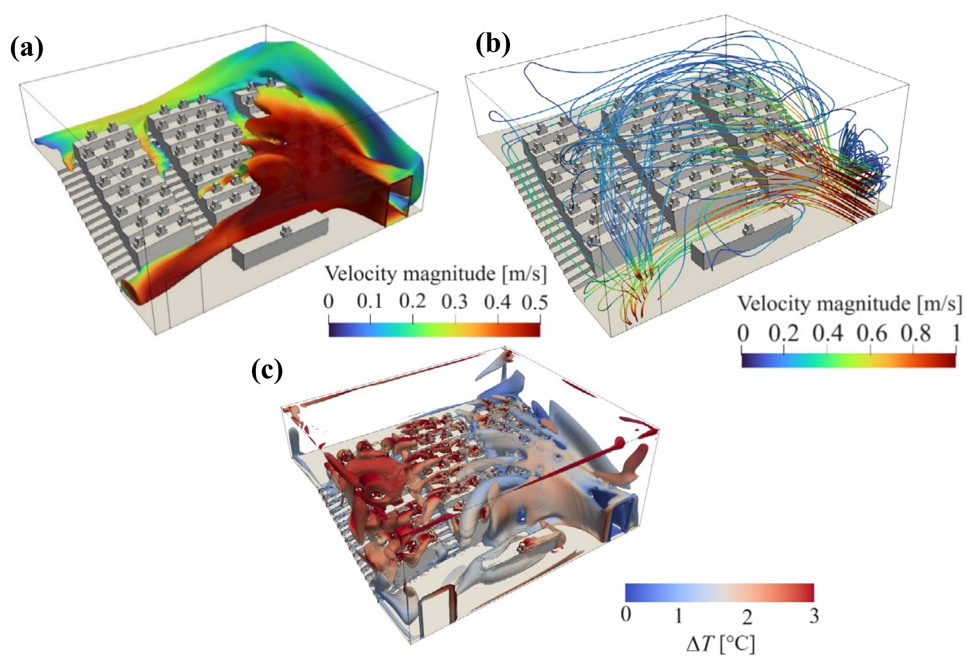

Fig. 3 "Mid-season" case $T_e = T_0 = 20$ °C, $U = 1.0$ m/s. **a** Iso-surface at $\Delta T = 1$ °C and **b** streamlines of the inlet flow, both colored with the velocity magnitude (please notice the different color scale in panels a,b). (c) selected iso-surfaces of the Q-criterion colored with the temperature deviation, ΔT

In summary, the upper-left part of the room is dominated by the convection induced by the occupants' thermal power, whereas, in the lower-right part of the amphitheater, the flow is dominated by the momentum flux due to the inlet jet, which tends to generate colder and horizontally orientated structures. However, the effectiveness of this mechanism depends on how the inlet jet penetrates inside the room and, in turn, on the inlet jet momentum and temperature. In the following, we study the effect of these external parameters on the fluid dynamics.

3.2 Effect of the external ventilation and temperature

3.2.1 Effect of the external ventilation

Figure 4 shows the case of low inlet velocity ($U = 0.5$ m/s) with the "mid-season" external temperature $T_e = T_0$. The incoming fresh-air momentum is not high enough to break thermal stratification. Hence, the fresh air generates a small-section, high-velocity stream tube that remains at the ground floor level short-circuiting the inlet and outlet doors (Fig. 4a, $\Delta T = 1$ °C iso-surface colored with velocity magnitude) without involving the remaining room volume.

In the entire volume above the height of the first desk row, the temperature deviation ΔT thus exceeds 3 °C (Fig. 4b, ΔT colormaps), i.e., a strong, stable, stratification. Therefore, the room can be roughly divided into two regions: a lower region, in the proximity of the teacher's desk, where external ventilation is intense and the temperature is not much higher than T_e (horizontal section in Fig. 4c), and an upper region, which instead presents very large and almost uniform values of temperature deviation, after a sharp transition at the level of the first tier (see the vertical section in Fig. 4c). Figure 4b corroborates this picture: all streamlines originating from the inlet door rapidly bend leftward, (x direction) and are directly connected to the outlet. In this configuration, the entire volume above the desks is dominated by the plumes generated by the occupants' heat flux, which easily prevail over the low inflow momentum (Fig. 4d).

Figure 5 depicts the case of high external ventilation ($U = 1.25$ m/s), with the same "mid-season" external temperature as above. The scenario is rather different compared to the case of low inlet velocity since, in this case, the momentum from the inlet prevails over the buoyancy generated by the occupants in most of the room. Only a small fraction of the inlet flow remains at the ground floor level and heads directly to the outlet: most of

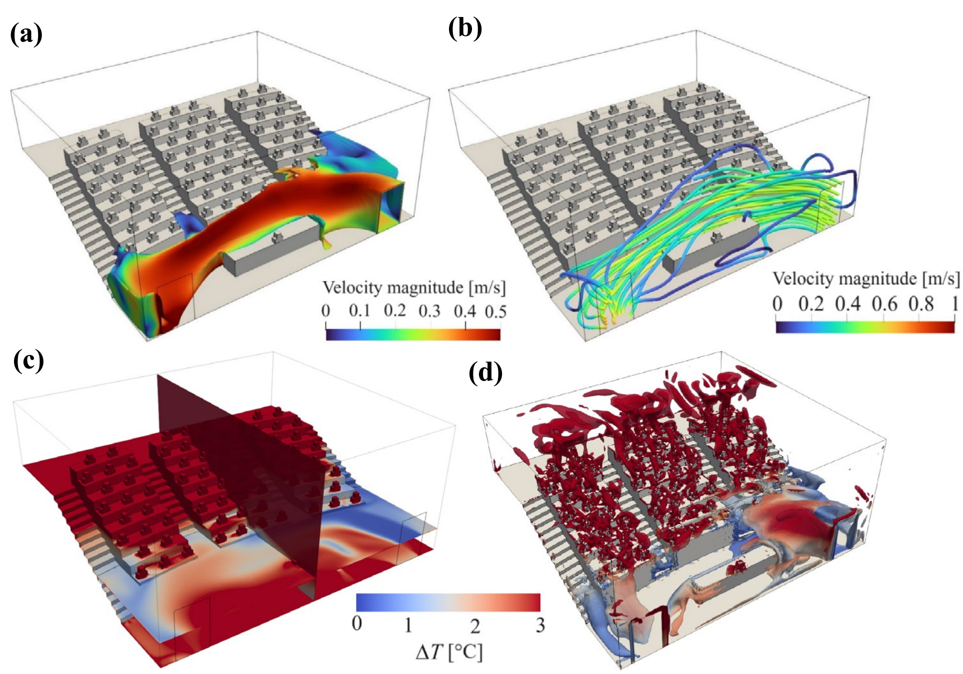

Fig. 4 Effect of reducing the inlet velocity down to $U = 0.5$ m/s for the "mid-season" case, $T_e = T_0$. **a** iso-surface at $\Delta T = 1$ °C and **b** streamlines originating from the inlet door, both colored with velocity magnitude (please notice the different scale in panels a, b); **c** color maps of ΔT at the boundaries, on a vertical mid-plane, and a horizontal plane located 1 m above the ground floor; **d** selected iso-surfaces of the Q-criterion colored with the temperature deviation, ΔT

 https://doi.org/10.1007/s11012-026-02147-x

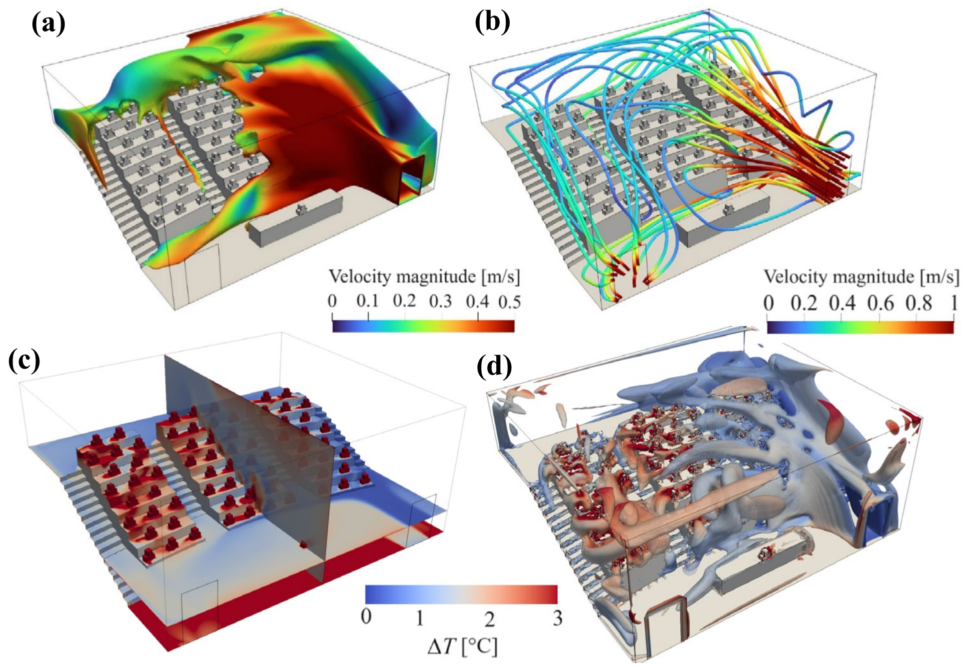

Fig. 5 Effect of increasing the inlet velocity up to $U = 1.25$ m/s for the "mid-season" case, $T_e = T_0$. **a** iso-surface at $\Delta T = 1$ °C and **b** streamlines originating from the inlet door, both colored with velocity magnitude (please notice the different scale in panels a, b); **c** color maps of ΔT at the boundaries, on a vertical mid-plane, and a horizontal plane located 1 m above the ground floor; **d** selected iso-surfaces of the Q-criterion colored with the temperature deviation, ΔT

the incoming air spreads over the sloping tiers, among the occupants, while the remaining portion runs along the right wall and then propagates in the space behind the desks, as described by the $\Delta T = 1$ °C iso-surface (Fig. 5a) and the path of the streamlines (Fig. 5b). The temperature observed in the vertical slice of Fig. 5c is more uniform, compared to the case $U = 0.5$ m/s, though it exhibits a significant temperature increase in the proximity of the ceiling, which is the signature of a remaining stratified layer. A region of low temperature above the stairs and the desks (aligned with the y axis) highlights the propagation of the inlet jet toward the highest rows in the right part of the room (Fig. 5c). Similarly to the reference case, the lower temperatures are mostly localized in the region behind the tiers and in front of the inlet. The streamlines (Fig. 5b) also present similarities with the reference case, with a recirculation zone above the teacher's desk and on the right of the inlet. Buoyant plumes from occupants' heating develop only in the upper-left part of the hall, where the momentum of the incoming flow is weaker (see the Q-criterion iso-surfaces colored with temperature deviation in Fig. 5d). In the remaining part of the room, the high velocities completely disrupt the coherence of thermal plumes, and the flow is dominated by horizontal vortices with axes parallel to the desk rows, associated with relatively low ΔT. It is interesting to note that, though the resulting pattern is sensitive to the propagation of the inlet jet inside the room, these features persist even if the heat flux from the occupants is decreased, as briefly shown in Appendix C.

3.2.2 Effect of the external temperature

In addition to the "mid-season" cases at different inflow velocities, we also investigate the role of external temperature. In Fig. 6, we show the effect of lowering the external temperature by 10 °C ($T_e = T_0 - 10$ °C $= 10$ °C), while keeping the inlet velocity to the reference value $U = 1$ m/s. We can assume this as a "winter" condition. Compared to the "mid-season" case, a lower temperature has the effect of confining a significant portion of the inflow to the lower-front part of the amphitheater, at the teacher's desk level. A well-defined high-velocity stream-tube is generated, and directly connects the inlet with the outlet door (Fig. 6a). The vertical temperature map, shown in Fig. 6c, depicts a significant thermal stratification.

Consistently, close to the ceiling, a quite independent flow characterized by a large-scale, slow, recirculation develops, as shown by the streamlines in Fig. 6b. Therefore, similarly to the low inlet velocity case ($U = 0.5$ m/s),

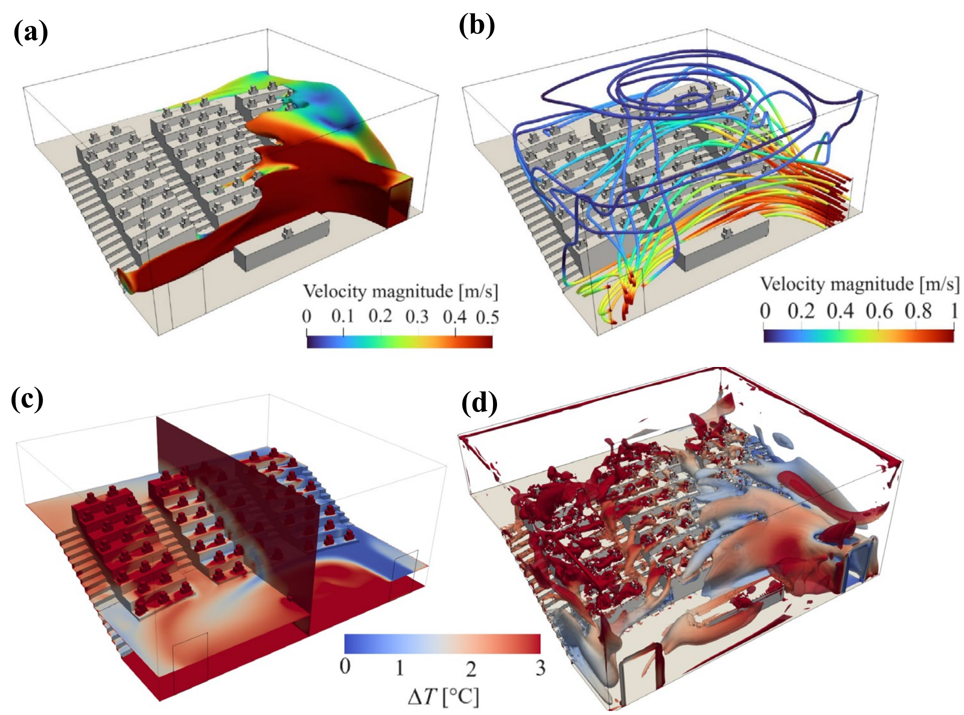

Fig. 6 Effect of the external temperature on the inlet jet propagation. Winter case: $T_e = 10$ °C. **a** iso-surface at $\Delta T = 1$ °C and **b** streamlines originating from the inlet door, both colored with velocity magnitude (please notice the different scale in panels a, b); **c** colormaps of ΔT at the boundaries, on a vertical mid-plane, and a horizontal plane located 1 m above the ground floor; **d** selected iso-contours of the Q-criterion colored with the temperature deviation ΔT

the room is divided into two regions: the upper-left region dominated by the occupants' buoyant plumes, and the right-lower region dominated by the momentum of the incoming air. The scenario is confirmed by the Q-criterion iso-surfaces (Fig. 6d) showing several buoyant plumes above the upper-left occupants, and the horizontal advective structures in the right-lower part of the amphitheater. Conversely, the higher inflow temperature of the summer case ($T_e = T_0 + 10$ °C = 30 °C, Fig. 7) allows for the warm inlet air to propagate toward the upper part of the room, breaking thermal stratification (Fig. 7c). In this case, the stream-tube short-circuiting inlet and outlet doors is not present, and the incoming air mixes throughout the whole room volume (Fig. 7a).

Accordingly, the streamlines shown in Fig. 7b give evidence of a single recirculating pattern that involves both the lower and upper layer of the room volume, in analogy with the high inlet velocity case. The Q-criterion iso-surfaces highlight that the right part of the amphitheater is dominated by the horizontal advective structures, driven by the momentum of the inlet jet, and involving the entire room height. In contrast, in the upper left part, warm structures that result from the interaction of the inlet momentum flux with the occupants' heat flux dominate. In summary, the structure of the velocity and temperature fields is also influenced by the temperature of the inlet jet. Higher external temperatures promote a more uniform (though higher) temperature in the room, preventing stratification in two regions both in the case of low external temperature and low inlet velocity. Amphitheater classrooms thus present different scenarios at different heights in terms of thermal comfort and ventilation efficiency. The presence of different, separated, flow regions may underlie consequences not only for thermal comfort design but also for the air quality in the room. These aspects will be discussed in the next sections.

3.3 From fluid mechanics to thermal comfort

To evaluate the consequences of the structure of the flow on the comfort of the occupants, we use the PMV/PPD method defined by the ASHRAE Standard 55–2004 [15] to describe the local thermal comfort, whose computation is here performed by functions available in OpenFOAM®. The left column of Fig. 8 shows the effect of the inlet velocity on PMV in the case $T_e = T_0$, corresponding to mid-season conditions (accordingly, we assumed an occupants' clothing insulation factor equal to 0.75 clo = 0.116 m^2 K/W), while in the right column of Fig. 8 are reported the percentages of dissatisfied (PPD). With the lower inflow rate ($U = 0.5$ m/s, Fig. 8a), the comfort

 https://doi.org/10.1007/s11012-026-02147-x

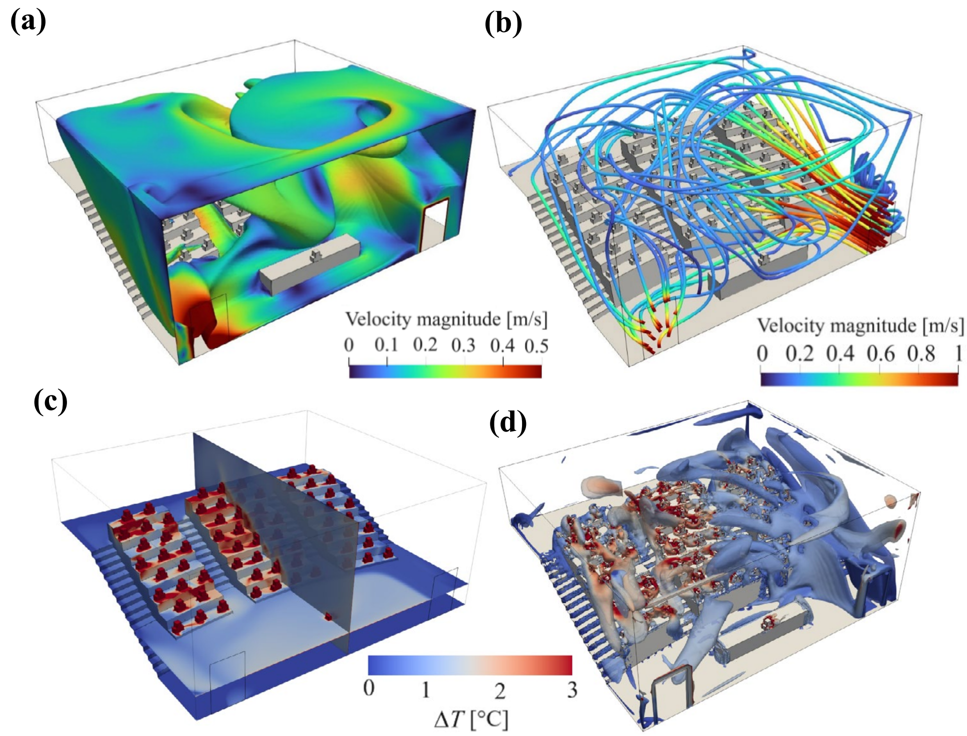

Fig. 7 Effect of the external temperature on the inlet jet propagation. Summer case: $T_e = 30$ °C. **a** iso-surface at $\Delta T = 1$ °C and **b** streamlines originating from the inlet door, both colored with velocity magnitude (please notice the different scale in panels a, b); **c** colormaps of ΔT at the boundaries, on a vertical mid-plane, and a horizontal plane located 1 m above the ground floor; **d** selected iso-contours of the Q-criterion colored with the temperature deviation ΔT

distribution is mainly affected by thermal stratification, and the region at the ground floor level in the vicinity of the teacher's desk is the sole exhibiting PMV values that indicate good comfort (about in the range -1, 1). Conversely, the whole upper volume of the room is not reached by the fresh air and suffers from high temperatures due to the stratification, thus resulting in PMV > 2, i.e., a quite warm sensation. Therefore, cool sensation and good comfort are limited to the close neighborhood of the doors due to the fresh air ventilation from the door (Fig. 4a and b). Similarly, the predicted percentage of dissatisfaction (PPD, Fig. 8d), namely the percentage of people not comfortable in their activity, is low at the ground level around the teacher's desk but grows in front of the doors and moving towards the back desk rows of the amphitheater.

A higher inlet velocity (Fig. 8 b, $U = 1.0$ m/s) changes this scenario, mainly because the momentum of the inlet jet prevents thermal stratification of the room air. Globally, the PMV remains about small values, though a slight cool is perceived by the persons directly impacted by the incoming jet in the lower right seats. This is the only region where the PPD attains significant values (Fig. 8e). A further increase in the inlet air speed ($U = 1.25$ m/s, Fig. 8c, f) preserves the above scenario, with a slightly higher percentage of occupants that perceive slight cool (Fig. 8c) and the high PPD region in the front of the inlet door (Fig. 8f).

In Fig. 9, we provide an overall quantitative and synthetic view of the comfort performance of the amphitheater classroom, which can be employed for preliminary design considerations. This figure presents the horizontally averaged temperature defect (left panel) and PPD (right panel) as functions of the height. The low inflow case ($U = 0.5$ m/s) is characterized by a strong, vertical temperature gradient that penalizes thermal comfort. Therefore, the corresponding PPD increases with height, reaching the highest percentages of dissatisfied people (blue dots in Fig. 9b). In the other two cases (mid and high inlet velocity), though the temperature defect increases to some extent with height, the average PPD decreases due to the decreasing effect of the air speed and, globally, remains limited to much lower values compared to the low inflow case.

In summary, in the low-velocity case, the inlet jet momentum is not able to break thermal stratification and the steep increase in the mean temperature penalizes thermal comfort in the upper part of the room. Conversely, efficient ventilation can improve thermal comfort also at very large heights, thus promoting effective mixing throughout the room height. However, too strong ventilation may also be negative, as shown in Fig. 9b, where

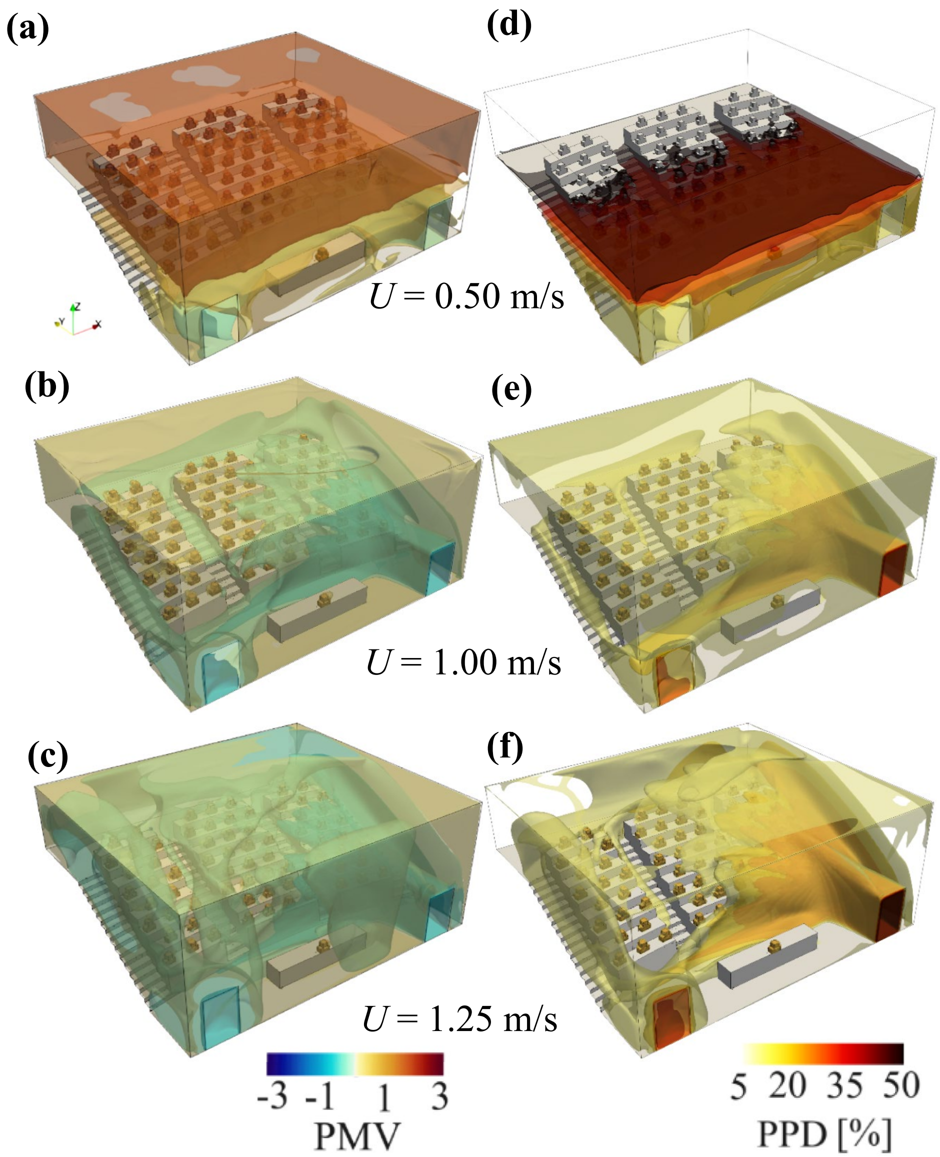

Fig. 8 Thermal comfort for $T_e = 20$ °C. Left column (**a**, **b**, **c**): Spatial distribution of Predicted Mean Vote (PMV); right column (**d**, **e**, **f**): Predicted Percentage of Dissatisfied. First row (**a**, **d**): $U = 0.5$ m/s, middle row (**b**, **e**): $U = 1.0$ m/s, lower row (**c**, **f**): $U = 1.25$ m/s

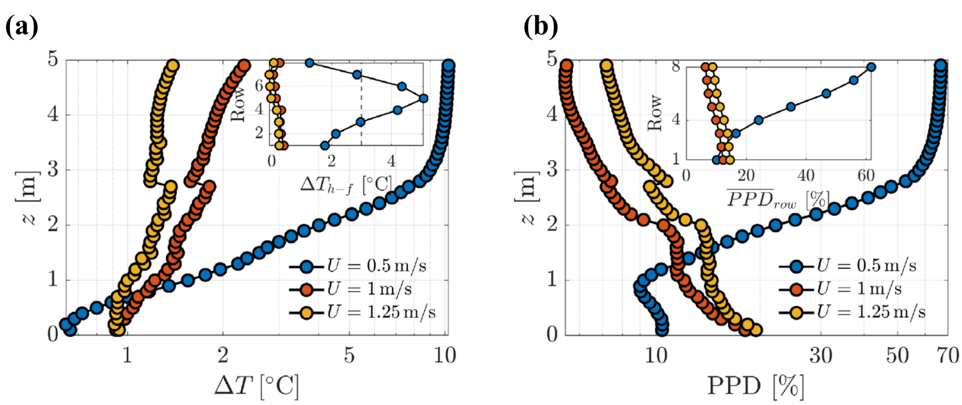

Fig. 9 Thermal comfort for $T_e = 20$ °C and different inlet velocities. Horizontal average of the temperature defect ΔT (panel a) and PPD (panel b) as functions of the height. The insets show **a** the head-to-foot temperature difference for the different rows and **b** the mean PPD value over a 1 m vertical interval at the height of each row. Blue circles indicate the case $U = 0.5$ m/s, red circles indicate $U = 1.0$ m/s, and yellow circles indicate $U = 1.25$ m/s

 https://doi.org/10.1007/s11012-026-02147-x

the overall PPD presents a non-monotonous behavior with U. Furthermore, temperature profiles provide an approximate estimate of the variations over the seated occupied region. Following ASHRAE Standard 55 for seated occupants, we considered a 1 m vertical interval between foot and head level [56]. The differences were computed as head-level minus foot-level values and are shown in Table 1. For U = 0.5 m/s, the foot-to-head temperature difference exceeds 3 °C in the central rows, where the difference is maximum. Conversely, for U = 1.0 m/s and U = 1.25 m/s, the corresponding differences remain below about 0.4 °C. This confirms that vertical thermal variations are relevant in the low-velocity stratified case, especially at the interface between the ventilated and the stratified regions, whereas larger inlet velocities suppress the seated vertical temperature gradient.

In conclusion, tailoring the inlet jet penetration through the room via temperature and velocity can be an effective tool for optimizing thermal comfort over the entire amphitheater volume. Unsurprisingly, the most important parameter to set ventilation seems to reside in the total heat flux emitted by the occupants. We demonstrated that, despite employing refined integral indices, 3D visualization with Q-criterion with temperature may already give faithful preliminary design considerations, being an excellent candidate to be employed for systematic, comparative, analyses. In addition, we quantified that, for the present boundary conditions, an inlet wind of about 1 m/s is needed. In Appendix C, due to the reduced heat flux from the occupants, this velocity is of order 0.5 m/s. These considerations can find applications in physically-inferred systematic tools for evaluation of ventilation, possibly informed with a relatively computationally affordable simulations such as the ones performed here. Such a model may assess the ventilation through classical integral indices or with automatic image analyses tools of the relevant structures such as the ones proposed in Fig. 7.

4 Results: air quality

The Age of Air q is a steady quantity that measures the time needed for the external air to reach and bring fresh air to a given location and quantifies the ventilation efficiency in indoor environments [13]. The spatial distribution of the Local Mean Age of Air (LMA) allows one to define a time-independent index describing the behavior of a passive scalar and infer the air quality in the different zones of the indoor environment and, consequently, design strategies to improve the air quality in the most sensitive regions.

It should be mentioned that, in a well-mixed box with initial uniform concentration and subjected to external ventilation, the Mean Age of Air coincides with the time needed for the volume-average concentration defect to decrease to the value $1/e$. The definition of the Age of Air allows for a dual interpretation of the results. If pollutants are introduced from the inlet, areas with a lower age of air will be the most polluted. Conversely, if fresh air is supplied from outside, regions with a higher age of air will experience poorer air quality. For the sake of clarity, in the following, we interpret the results assuming that fresh air is supplied from the inlet.

In Fig. 10, we present the LMA, q. First, we consider the effect of the inlet velocity in the mid-season thermal conditions. As discussed above, at low velocity, thermal stratification dominates (Fig. 4). Consequently, the

Table 1 Estimated head-to-foot temperature differences at different rows, for $T_e = 20$ °C

Row	z_{head} [m]	Temp. difference, U = 0.5 m/s [˚C]	Temp. difference, U = 1.0 m/s [˚C]	Temp. difference, U = 1.25 m/s [˚C]
1	1.48	1.77	0.40	0.25
2	1.82	2.14	0.30	0.23
3	2.16	2.97	0.27	0.23
4	2.50	4.21	0.31	0.16
5	2.84	5.08	0.14	-0.03
6	3.18	4.36	0.10	-0.07
7	3.52	2.85	0.05	-0.09
8	3.90	1.26	0.26	0.06

upper portion of the room behaves differently from the lower one, reaching the highest values of LMA among the explored conditions, as apparent in Fig. 10b. Approximately from mid-height above, the volume is split into a central region of intermediate LMA and two lateral regions with larger values. Conversely, in the lower portion of the room as well as in the proximity of the doors, the previously observed direct ventilation (Fig. 4) leads to significantly lower LMA values. Stratification is particularly relevant because of the amphitheater structure of the classroom. As a matter of fact, in this condition, occupants sitting at the higher desk rows are potentially exposed to poor air quality even in the presence of a stream of fresh air. As velocity increases to $U = 1.0$ m/s (Fig. 10c) and thermal stratification is inhibited by the higher momentum influx, uniformly lower values of LMA are observed, although a region of relatively higher LMA is found in the upper left part of the room, which is excluded by the main inlet ventilation flow. A further increase in the inlet velocity (Fig. 10d) reduces the LMA and the peak values, though lower compared to the previous cases, are localized close to the recirculating vortex above the teacher's desk, observed in Fig. 3.

Subsequently, we examine how the temperature of the inlet jet influences the LMA within the room. In the winter conditions ($T_e = 10$ °C, Fig. 10a), the almost horizontal iso-surfaces of LMA at large heights depict the inability of the cold, incoming jet to reach the upper portion of the room volume, as depicted also by Fig. 6. However, the

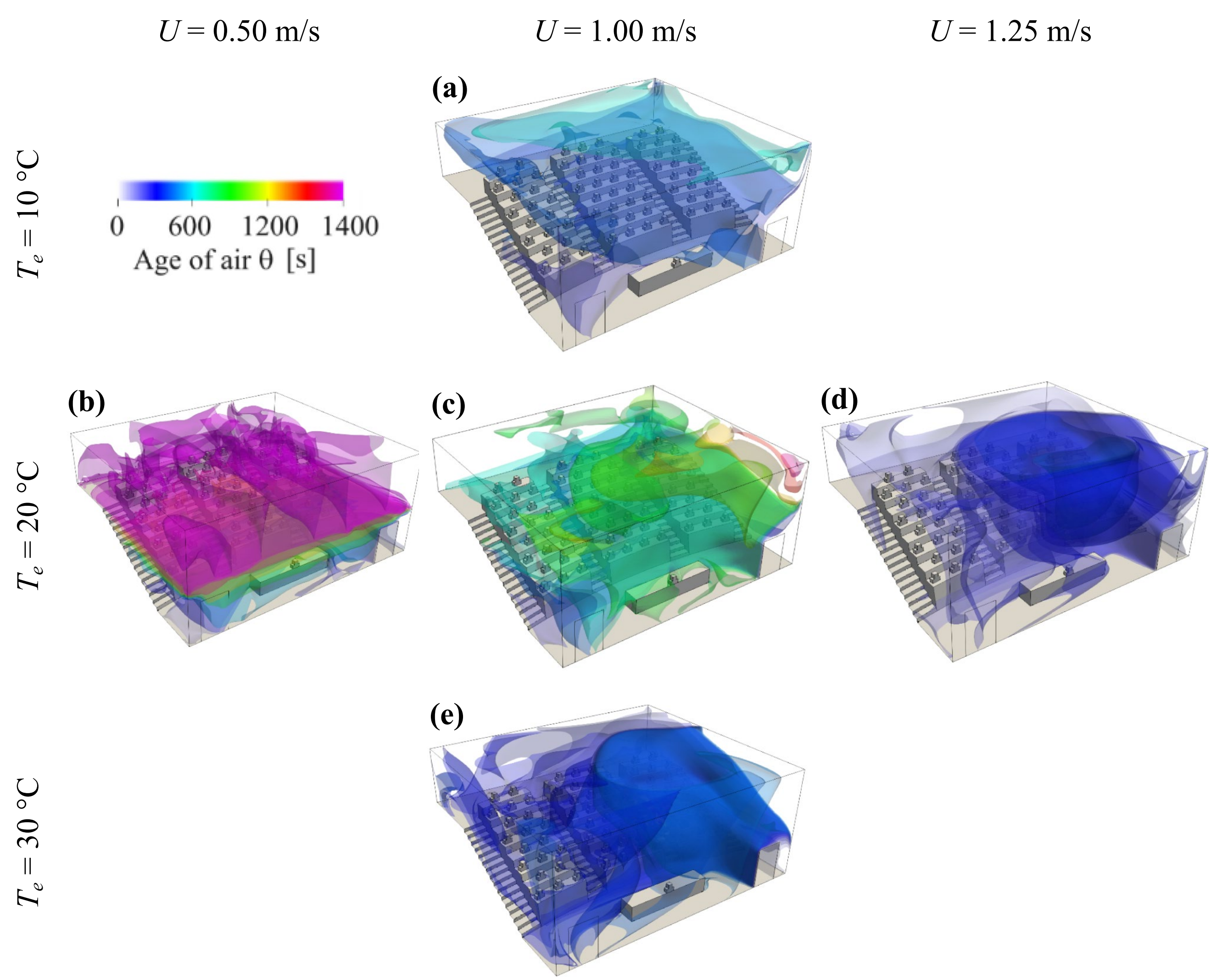

Fig. 10 Spatial distribution of the local mean age of air q for varying inlet jet velocity and external temperature, visualized through iso-surfaces

 https://doi.org/10.1007/s11012-026-02147-x

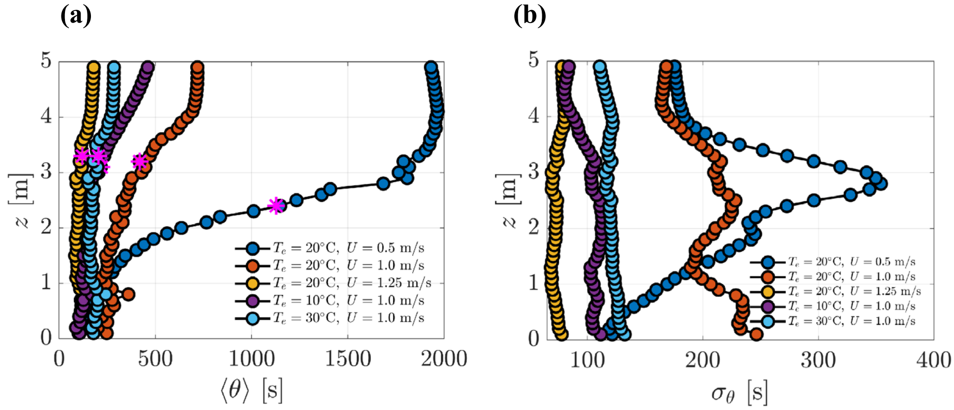

Fig. 11 Horizontally averaged values of the LMA, q, as a function of the height: **a** average and **b** standard deviation over the horizontal planes. The magenta stars indicate the average AOA of the whole room

Table 2 Volume averaged LMA within the whole room, for the considered cases

	U = 0.50 m/s	U = 1.00 m/s	U = 1.25 m/s
T_e = 10 °C		220 s	
T_e = 20 °C	1125 s	421 s	121 s
T_e = 30 °C		204 s	

LMA is globally much smaller compared to the low velocity. Conversely, as shown in Fig. 7, increasing the inflow temperature to summer conditions (T_e = 30 °C) allows for increased mixing over the whole volume (Fig. 10e). This leads to the lowest LMA among the explored cases, with the only region of relatively high LMA due to the recirculating vortex located on the left of the inlet door.

In analogy with the previous section, these data are summarized into integral quantities by averaging the LMA on horizontal planes at different heights, as shown in Fig. 11 (with the volume average reported with stars and in Table 2), together with the standard deviation on each horizontal plane to give an insight on the spatial inhomogeneity.

Figure 11 indicates that, in general, both a higher temperature and larger inlet velocity promote vertical homogeneity. However, the effect of the inlet velocity is the most important. The comparison with the vertical temperature deviation profiles shown in Fig. 9a provides evidence that thermal stratification drives the behavior of the surface-averaged LMA. In agreement with Fig. 10, the highest values are observed in the upper part of the amphitheater, irrespective of the case considered. In the upper portion of the room volume, in the case of mid-season thermal conditions and low inflow velocity (blue circles in Fig. 11b), the surface-averaged LMA attains values that are more than twice compared to the second worst case, namely the reference case (mid-season and intermediate inlet velocity, orange circles in Figs. 11a and b), which, surprisingly, yields higher age of air compared to the winter case (blue circles in Fig. 11a). The reason seems to lie in the fact that, with low inlet temperature, the thermal plumes generated by the occupants partially compensate for the low mixing promoted by the inflow momentum.

The lowest surface-averaged LMA values in the upper zone amphitheater are observed for high inflow velocity or temperature (yellow circles in Figs.11a and b). The average age of air in the whole room (magenta stars in Fig. 11) decreases when increasing the ventilation intensity. At the same time, the low-velocity case is characterized by higher values of the standard deviation, while it decreases by about one-third when considering the highest velocity case due to a more effective mixing over the room volume.

5 Discussion and conclusion

We analysed the indoor fluid dynamics in an amphitheater classroom with the aim of assessing the effect of thermal stratification and mechanical ventilation on the comfort of the occupants and air quality. We considered a reference case, with the same internal and external temperature ($T_0 = T_e = 20$ °C) and an inlet velocity through a lower door, as high as 1.0 m/s. Then, we considered the effect of varying the air speed and temperature of the inflow separately. Due to the amphitheater shape of the classroom, the occupants were distributed over the height of the room, differently from what happens in a typical flat floor classroom. The effect of vertical stratification was crucial for the occupants' health and comfort.

The effectiveness of the ventilation results from the interaction between momentum and buoyancy fluxes. The former is due to the inflow velocity, whereas the latter depends on both the inflow temperature difference and heat flux generated by the occupants. The presence of the desk rows organized in tiers changes the fluid dynamics, leading to a much more effective resistance of the thermal plumes to break up and, at the same time, reduces the air quality in the upper tiers. The buoyant convection affects the spatial distribution of pollutants, showing that the exposure to better air quality of the occupants sitting in different regions depends on several factors, thus calling for a better understanding of how the geometrical parameters, such as the slope of the tiers, influences the fluid dynamics. Also, we observed that temperature fields were correlated with the Age of Air, thus suggesting that local monitoring of temperature could be an efficient way to assess and optimize the room ventilation strategies.

In the studied cases, the main parameter affecting the overall performance of the room is the inlet air speed. High inlet velocity promotes fresh air penetration and spreading over the amphitheater desk rows and tends to disrupt the convective structures generated by the occupants (Fig. 5). The result is a good mixing through the room height with relatively low AOA and high thermal comfort (Figs. 9 and 11). However, this aspect is intertwined with draught feeling in the portions of the room with intense ventilation [30]. Conversely, low air speed at the inlet confines the external air flow to the lower layer of the room in the region of the teacher's desk (Fig. 4) and allows the heat from the occupants to generate a steep thermal stratification, leading to the highest AOA and lowest thermal comfort. In contrast, an increase in the ventilation intensity breaks the coherence of thermal convection and drastically reduces the Age of Air. Therefore, the air speed through the inlet is crucial in defining effective ventilation all over the amphitheater. Decreasing the inlet air temperature tends to confine the inlet jet to the lower part of the amphitheater. However, in our tests, the inlet jet momentum is enough to let the fresh air reach also the upper-rear part of the room in the front of the inlet (Fig. 6). Conversely, with a warm inlet jet, buoyancy and mechanical ventilation concur to promote the air mixing thus resulting in a lower and more uniform AOA over the room height (Fig. 11a).

These aspects should be considered in the design phase of room ventilation, especially in the present case where thermal gradients are important due to the amphitheater structure of the room. Small jet penetration promotes better air quality (i.e. low Age of Air) in the central part of the sloping desk rows, while large jet penetration results in a lower AOA in the rear and lateral parts of the room, for the present configurations. Temperature deviation, ΔT, and AOA fields appear to be related. Therefore, temperature deviations, easier to measure, would give fruitful insight on the ventilation effectiveness and could be usefully employed to preliminarily assess ventilation strategies, within the perspective of ensuring better indoor air quality. The correlations between thermal comfort and air quality need to be further explored and quantified to propose effective guidelines for blended analyses.

This work is intended as a fluid mechanics building block toward a systematic understanding of the role of stratification and ventilation in comfort and air quality within classrooms of considerable height. However, our analysis presents some limitations that are worth mentioning here. First, we considered the steady, RANS, solution to the problem. Therefore, our work did not consider potential large-scale instabilities that can develop, especially in high-shear regions. The unsteadiness of the flow is known to improve mixing, erode stable stratification

[29] and reduce the extension of stagnation regions [57]. Thus, further extensions of this work may consider the unsteadiness of the flow, e.g., by Large Eddy Simulation. Similarly, we only considered one inlet/outlet condition, but other configurations could also be relevant. Also, we did not considered buoyant pollutants and their effects on the airflow, and we considered only the inlet as a source of pollutants or fresh air. From this point of view, further developments are required to assess CO_2 distribution within the room and fine particle matter dispersion from the occupants, to name a few. Within the presented framework, our findings may also be considered as a building block towards physics-aware models for air quality analysis based on blending physical understanding with data-driven methods [58], with the final goal of providing additional guidelines as well as practices to improve air quality and thermal comfort within educational indoor spaces of large height. Within this context, computationally affordable steady models such as the RANS approach employed here can be exploited as a first physics-informed tool, before moving toward more refined fluid-dynamics tools for systematic analyses. These models may analyse integral quantities but also visual representations of the field through specific algorithms, to optimize the spatial distribution of ventilation through simple image analysis techniques.

Appendix A: mesh convergence analysis

The mesh is generated through the utilities *blockMesh* and *snappyHexMesh* embedded in the OpenFOAM environment. The former is employed to create a background mesh of hexahedral elements, with a local refinement in the vicinity of the edges to better describe the flow features in these sharp corners of the external geometry (see Fig. 12a). Thanks to a STL file of the geometry of the desks, stairs and occupants, *snappyHexMesh* generates the boundary elements as well as their refinements. We consider three successive refinements in the vicinity of the surfaces. To improve the quality of the resulting mesh, we added at the walls three boundary layers with an expansion ratio of 1.2. Mesh convergence is assessed by varying the background mesh through the utility *blockMesh* without varying the boundary refinements so that the mesh is uniformly refined. We further verified that the resulting mesh satisfies typical geometrical requirements for a well-behaved simulation. The numerical implementation relies on employing second-order in space numerical schemes for all variables at play, including turbulent quantities. The solvers are set to a tolerance of 10^{-8} for all variables, except the pressure field which presents a tolerance on the last iteration of 10^{-7}. The numerical set-up allows for a smooth convergence from a zero solution to constant residuals and local quantities for all considered simulations, see Fig. 12(b, c, d, e). The convergence of the solution through the *buoyantBoussinesqSimpleFoam* algorithm is verified by monitoring the initial residuals as well as local values of six different probes located within the room. For all simulations reported in this work, we verified that all quantities in all considered points reach a constant value (with a tolerance of 1%) with initial residuals that fall below 10^{-4} for all quantities at play, except for pressure whose residual must fall below 10^{-3}. The mesh independence of the presented results is assessed for average quantities as well as through comparison of vertical velocity magnitude and temperature profiles in different, relevant, zones of the room. Three different refinements are considered by progressively increasing the background resolution, labeled as coarse (550′709 elements), intermediate (975′396 elements) and refined (1′397′695 cells).

In Table 3, we report the variation of average velocity magnitude and temperature in the whole domain, at the outlet and at two horizontal sections located at a height of 1 and 3 m. In all cases, results vary within a tolerance of order 0.01 m/s and 0.1 °C, thus suggesting that the presented results are not influenced by the mesh refinement, in terms of average quantities. In addition, we analysed several velocity magnitude profiles at relevant vertical lines to further assess the independence of the presented results in terms of local quantities (Fig. 13). The three

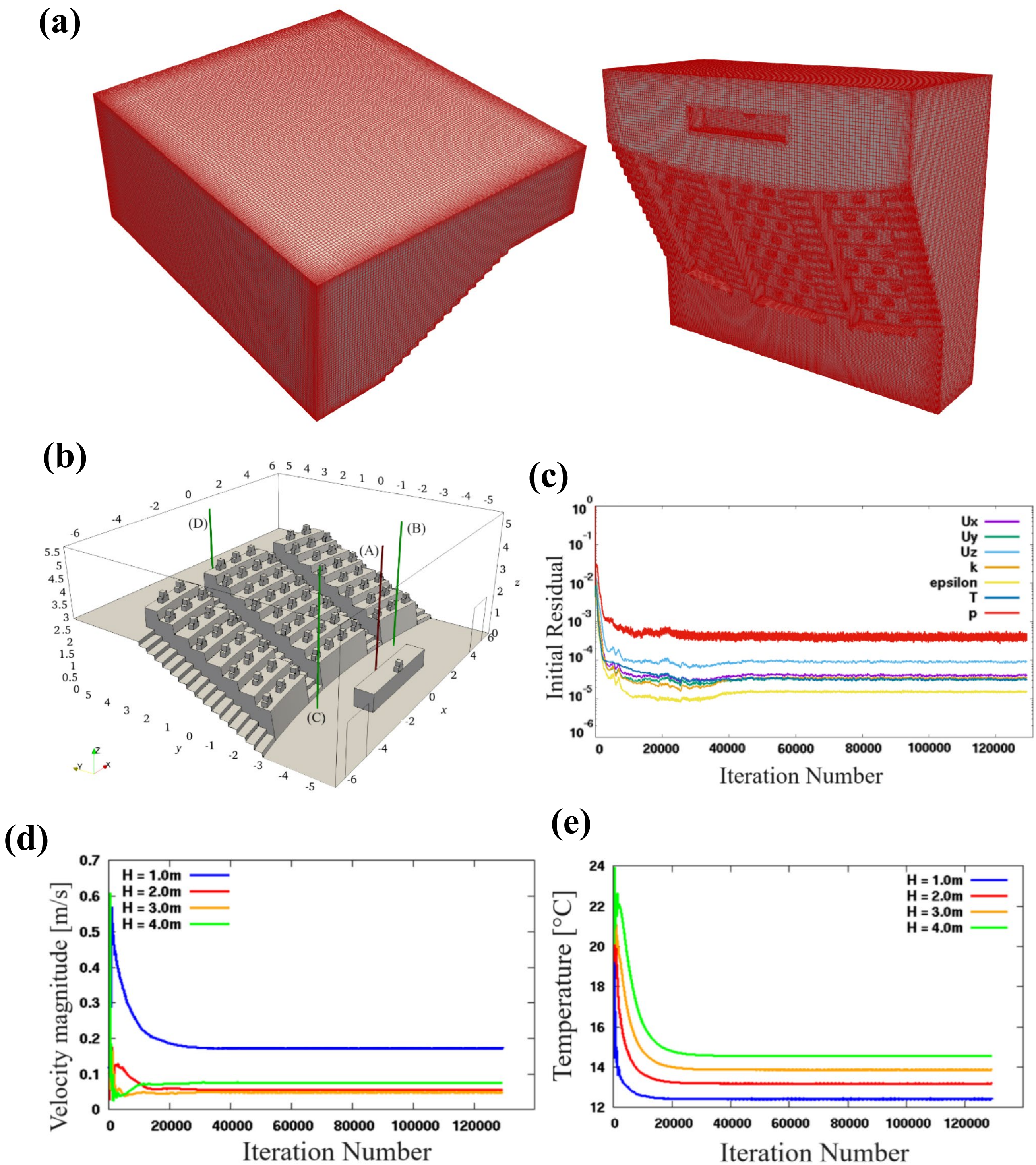

Fig. 12 **a** overview of the mesh employed in the present work; **b** sampling lines employed in the convergence analysis. Examples of convergence trends: **c** initial residuals, **d** velocity magnitude, **e** temperature, sampled at four points along the height of line (A) of panel (b)

 https://doi.org/10.1007/s11012-026-02147-x

Table 3 Average values of velocity magnitude and temperature for case $U=1.0$ m/s and $T_e=T_0$, in the whole domain, at the outlet and at two horizontal sections at different heights

Location of the average	Vel. Mag Coarse [m/s]	Vel. Mag Intermediate [m/s]	Vel. Mag Refined [m/s]	Temperature Coarse [°C]	Temperature Intermediate [°C]	Temperature Refined [°C]
Domain	0.2081	0.1877	0.2017	21.689	22.020	21.864
Outlet	1.0634	1.0659	1.0517	21.616	21.632	21.627
z = 1 m	0.0511	0.0518	0.0575	21.192	21.371	21.224
z = 3 m	0.0872	0.0836	0.0818	21.516	21.693	21.661

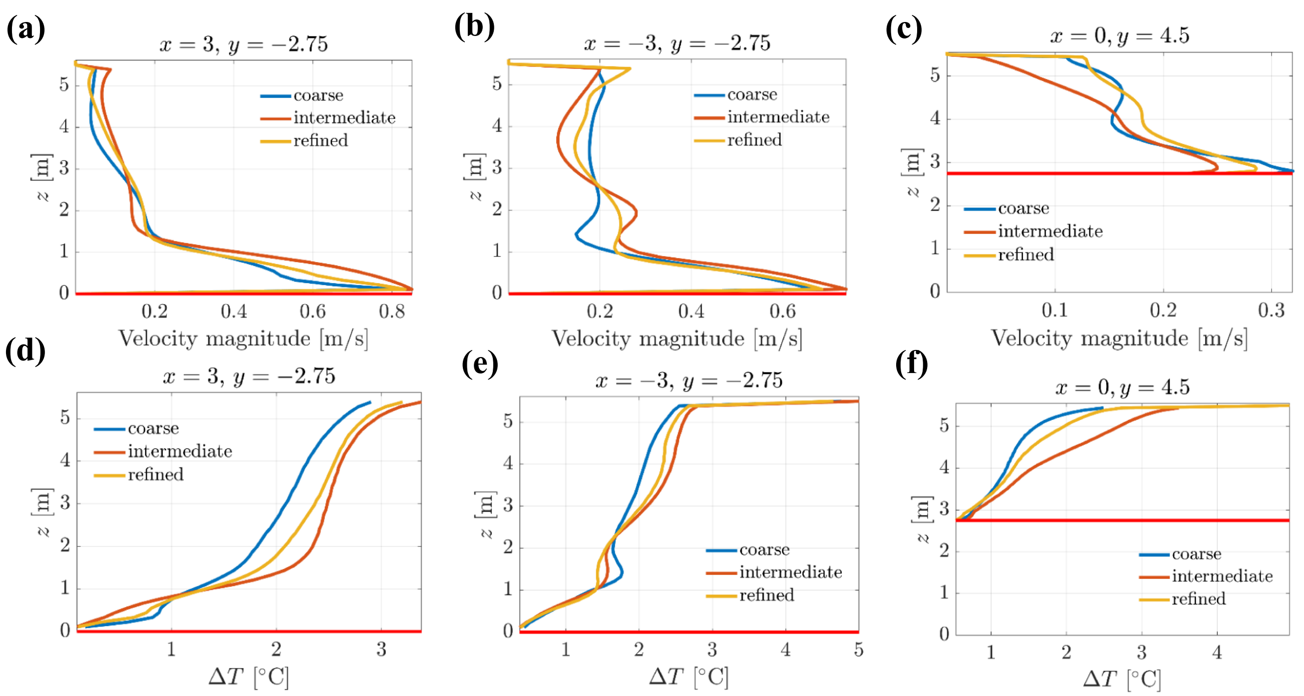

Fig. 13 Case $U=1$ m/s and $T_e=20$ °C. **a**, **b**, **c** Velocity and **d**, **e**, **f** and temperature profiles along vertical lines at coordinates indicated by the title, for the three different mesh refinements: (**a**, **d**) line (B) of Fig. 12, (**b**, **e**): line (C) of Fig. 12, (**c**, **f**): line (D) of Fig. 12. The red line denotes the local floor position

considered lines assess the convergence of the flow in the central and front part of the room close to inlet and outlet, and in the rear part of the room.

All considered profiles well match, in particular the intermediate and refined mesh ones. Although the error slightly increases for local quantities since also due to sampling differences, it remains of the same order of the average ones (10^{-2} m/s and 10^{-1} °C), thus suggesting that the presented results, focused on the flow structures and integral quantities, are mesh independent. In the present work, we employed the refined mesh.

Appendix B: validation of the numerical model

In this section, we report the validation of our implementation in terms of solvers and boundary conditions against the benchmark case of airflow in a rectangular cavity (of height H = 0.127 m along the Z direction, width W = 0.582 m along the Y direction, and length L = 0.372 m along the X direction) with heated floor, reported in Fig. 14. Air at fixed temperature is injected from a slot on the top left while the outlet is located on the bottom right; at the same time, the bottom boundary emits a constant thermal power while other walls are adiabatic.

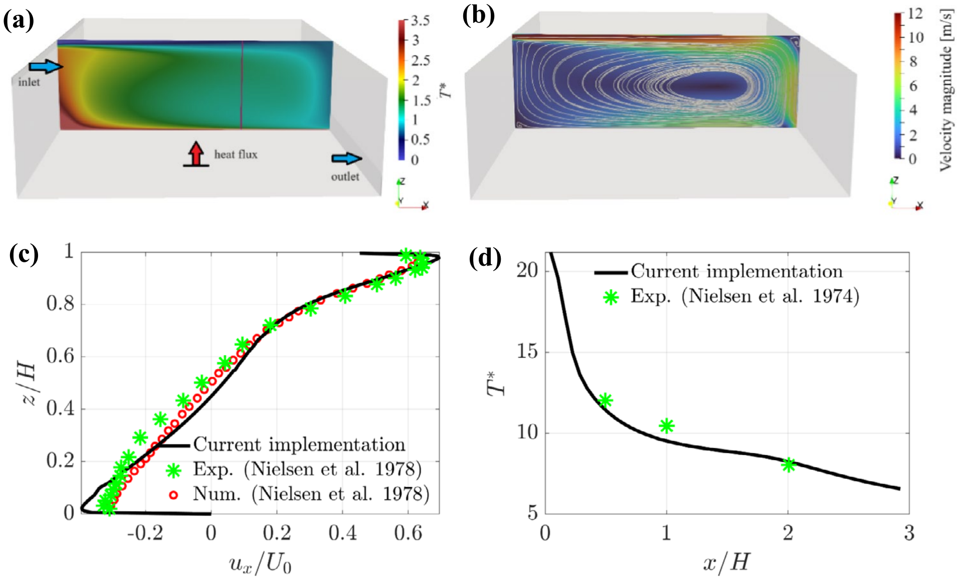

Fig. 14 **a**, **b** Numerical setup with inlet, outlet and heat flux boundary conditions, overlaid with colormaps of (**a**) normalized temperature $T^*=(T\text{-}T_0)\ /\ |T_e\text{-}T_0|$, where $T_e=23.6$ °C is average outlet temperature, and (**b**) velocity rescaled with the inlet one U_0, sampled at the center along the spanwise direction (Y). Panel (b) also reports the streamlines of the velocity field. **c** Streamwise velocity sampled as a function of Z along the line with coordinates $(x, y)=(2H—L/2, 0)$ (magenta line in panel (a): current implementation (black line) against experimental (green stars) and numerical (red circles) results of Nielsen et al. [59]. **d** Normalized surface temperature as a function of x sampled along the line with coordinates $(y, z)=(0.67\ W, 0)$: current implementation (black line) against experimental (green stars) results of Nielsen [60]

Our numerical results are compared against the experimental and numerical results extracted from Nielsen et al. [59] in terms of velocity, and against the experimental results of Nielsen [60] in terms of surface temperature. For our purposes, we note that we employed the same set-up, boundary conditions and physical parameters reported in Nielsen et al. [59, 60]: the inlet mean velocity is $U_0=15.2$ m/s with a turbulence intensity of 5% and constant inlet temperature $T_0=22$ °C. A uniform heat flux of 128 W is imposed at the bottom while other walls are adiabatic. Results show a good agreement and ensure that our implementation is correct both for velocity and temperature fields, thereby validating our numerical method, whose independence of the presented results with the mesh size has already been demonstrated.

Appendix C: effect of the ventilation velocity with a lower heat source from the occupants

As a matter of example, Fig. 15 shows the flow patterns developing for different ventilation intensity and fixed external temperature equal to the internal one $T_e=T_0=20$ °C when a different total power is emitted from the occupants, here equal to 23 W while all other conditions remain unchanged. Flow structures appear very similar to the ones exposed in the main text, suggesting that the described features are robust and likely develop in a large range of occupants' heat transfer conditions, for the considered ventilation configuration.

 https://doi.org/10.1007/s11012-026-02147-x

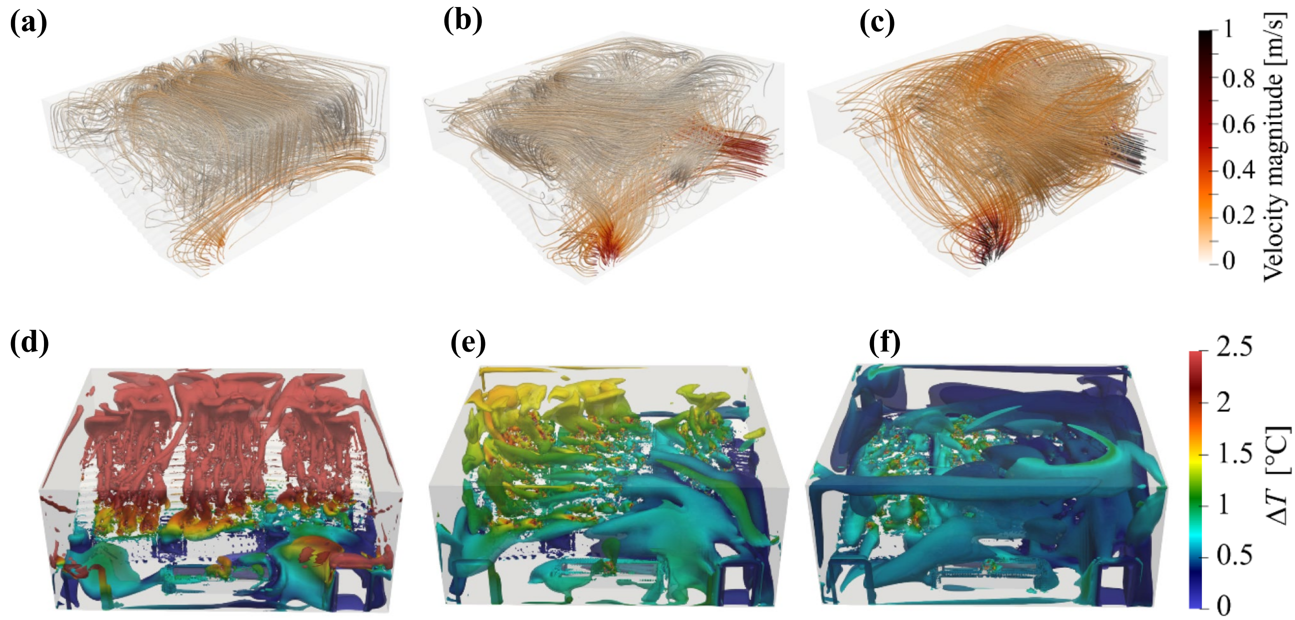

Fig. 15 **a**, **b**, **c** Velocity streamlines and **d**, **e**, **f** iso-surfaces of Q-criterion colored with the temperature difference with respect to the external one, for increasing velocity and fixed total heat flux from the occupants lowered as low as 23 W

Acknowledgements This study was partially supported by the Italian workers' compensation authority, Istituto Nazionale Assicurazione e Infortuni sul Lavoro (INAIL) within the Research Activity Plan 2019-2021. The authors are grateful to F. Angius for the helpful discussions about the initial formulation of the numerical model.

Author contributions P.G. Ledda: Writing—original draft, review and editing, Methodology, Conceptualization, Investigation, Formal analysis, Visualization. M.G. Badas: Writing—review & editing, Supervision, Conceptualization, Methodology, Formal Analysis. G. Querzoli: Writing—review & editing, Supervision, Methodology, Conceptualization, Visualization. P. Monti: Writing—review & editing, Supervision, Conceptualization. A. Pelliccioni: Writing—review & editing, Supervision, Conceptualization.

Funding Open access funding provided by Università degli Studi di Cagliari within the CRUI-CARE Agreement. Istituto Nazionale per l'Assicurazione Contro Gli Infortuni sul Lavoro.

Data availability The data that support the findings of this study are available from the corresponding author upon reasonable request.

Declarations

Conflict of interest The authors have no conflicts to disclose.

References

1. Bernstein JA, Alexis N, Bacchus H, Bernstein IL, Fritz P, Horner E, Li N, Mason S, Nel A, Oullette J, Reijula K, Reponen T, Seltzer J, Smith A, Tarlo SM (2008) The health effects of nonindustrial indoor air pollution. J Allergy Clin Immunol 121(3):585–591
2. Ramanathan V, Feng Y (2009) Air pollution, greenhouse gases and climate change: global and regional perspectives. Atmos Environ 43(1):37–50
3. Sundell J (2004) On the history of indoor air quality and health. Indoor Air 14(s7):51–58
4. World Health Organization (2021) WHO global air quality guidelines: particulate matter (PM2. 5 and PM10), ozone, nitrogen dioxide, sulfur dioxide and carbon monoxide
5. Nazaroff WW (2023) Ten questions concerning indoor ultrafine particles. Build Environ 243:110641
6. Ren J, Wade M, Corsi RL, Novoselac A (2020) Particulate matter in mechanically ventilated high school classrooms. Build Environ 184:106986
7. Stamatelopoulou A, Asimakopoulos DN, Maggos T (2019) Effects of PM, TVOCs and comfort parameters on indoor air quality of residences with young children. Build Environ 150:233–244
8. Holmberg S, Chen Q (2003) Air flow and particle control with different ventilation systems in a classroom. Indoor Air 13(2):200–204
9. Hedge A, Erickson WA, Rubin G (1996) Predicting sick building syndrome at the individual and aggregate levels. Environ Int 22(1):3–19
10. Sundell J (1996) What we know, and don't know about sick building syndrome. ASHRAE J 38(6):51–57
11. Sandberg M, Sjöberg M (1983) The use of moments for assessing air quality in ventilated rooms. Build Environ 18(4):181–197
12. Remion G, Moujalled B, El Mankibi M (2019) Review of tracer gas-based methods for the characterization of natural ventilation performance: Comparative analysis of their accuracy. Build Environ 106180:106180
13. Sandberg M (1981) What is ventilation efficiency? Build Environ 16(2):123–135
14. Lidwell OM (1960) The evaluation of ventilation. J Hyg 58(3):297–305
15. Olesen BW (2004) International standards for the indoor environment. Indoor Air 14(s7):18–26
16. Arakawa Martins L, Soebarto V, Williamson T (2022) A systematic review of personal thermal comfort models. Build Environ 207:108502
17. ASHRAE (1992) Thermal environmental conditions for human occupancy ANSI/ASHRAE 55:5
18. E.W. Shaw (1972) Thermal Comfort: analysis and applications in environmental engineering, by P. O. Fanger. 244 pp. DANISH TECHNICAL PRESS. Copenhagen, Denmark, 1970. Danish Kr. 76, 50. Royal Society of Health Journal 92(3):164–164
19. Zhou B, Li Z, Yang B, Li X, Wang F, Wei S (2023) Thermal and draught perception in fluctuating stratified thermal environments with intermittent impinging jet ventilation. Build Environ 229:109934
20. Liu W, Zhang TT, Lai D (2023) Inverse design of a thermally comfortable indoor environment with a coupled CFD and multi-segment human thermoregulation model. Build Environ 227:109769
21. De Dear RJ, Brager GS, Reardon J, Nicol F (1998) Developing an adaptive model of thermal comfort and preference/discussion. ASHRAE Trans 104:145
22. Humphreys M, Nicol F, Roaf S, (2015) Adaptive thermal comfort: foundations and analysis. Routledge
23. Van Hoof J (2008) Forty years of Fanger's model of thermal comfort: comfort for all? Indoor Air 18(3):182–201
24. Van Hoof J, Schellen L, Soebarto V, Wong JKW, Kazak JK (2017) Ten questions concerning thermal comfort and ageing. Build Environ 120:123–133
25. Liu F, Zhang L, Luo Z, Zhang C, Qian H (2023) Interactions of exhaled buoyant jet flow and human motion-induced airflow: An experiment study in a water tank. Build Environ 242:110603
26. Gao N, He Q, Niu J (2012) Numerical study of the lock-up phenomenon of human exhaled droplets under a displacement ventilated room. Build Simul 5(1):51–60
27. Rim D, Novoselec A, Morrison G (2009) The influence of chemical interactions at the human surface on breathing zone levels of reactants and products. Indoor Air 19(4):324–334
28. Linden PF, Cooper P (1996) Multiple sources of buoyancy in a naturally ventilated enclosure. J Fluid Mech 311(1):177
29. Linden PF (1999) The fluid mechanics of natural ventilation. Annu Rev Fluid Mech 31(1):201–238
30. Toftum J (2004) Air movement - good or bad? Indoor Air 14(s7):40–45
31. Horikiri K, Yao Y, Yao J (2014) Modelling conjugate flow and heat transfer in a ventilated room for indoor thermal comfort assessment. Build Environ 77:135–147
32. Nielsen PV (2015) Fifty years of CFD for room air distribution. Build Environ 91:78–90
33. Raji A, Hasnaoui M, Bahlaoui A (2008) Numerical study of natural convection dominated heat transfer in a ventilated cavity: Case of forced flow playing simultaneous assisting and opposing roles. Int J Heat Fluid Flow 29(4):1174–1181
34. Rim D, Novoselac A (2010) Ventilation effectiveness as an indicator of occupant exposure to particles from indoor sources. Build Environ 45(5):1214–1224

35. Liu S, Novoselac A (2014) Lagrangian particle modeling in the indoor environment: A comparison of RANS and LES turbulence methods (RP-1512). HVAC&R Research 20(4):480–495
36. Chatzidiakou L, Archer R, Beale V, Bland S, Carter H, Castro-Faccetti C, Edwards H, Finneran J, Hama S, Jones RL, Kumar P, Linden PF, Rawat N, Roberts K, Symons C, Vouriot C, Wang D, Way L, West S, Weston D, Williams N, Wood S, Burridge HC (2023) Schools' air quality monitoring for health and education: methods and protocols of the SAMHE initiative and project. Developments in the Built Environment 16:100266
37. Hama S, Kumar P, Tiwari A, Wang Y, Linden PF (2023) The underpinning factors affecting the classroom air quality, thermal comfort and ventilation in 30 classrooms of primary schools in London. Environ Res 236:116863
38. Su W, Yang B, Melikov A, Liang C, Lu Y, Wang F, Li A, Lin Z, Li X, Cao G, Kosonen R (2022) Infection probability under different air distribution patterns. Build Environ 207:108555
39. Arpino F, Cortellessa G, D'Alicandro AC, Grossi G, Massarotti N, Mauro A (2023) CFD analysis of the air supply rate influence on the aerosol dispersion in a university lecture room. Build Environ 235:110257
40. Pelliccioni A, Monti P, Cattani G, Boccuni F, Cacciani M, Canepari S, Capone P, Catrambone M, Cusano M, D'Ovidio MC, De Santis A, Di Bernardino A, Di Menno A, di Bucchianico S, Di Renzi R, Ferrante A, Gaeta R, Gaddi M, Gherardi M, Giusto A, Gordiani L, Grandoni G, Leone G, Leuzzi N, L'Episcopo F, Marcovecchio A, Pini T, Sargolini F, Tombolini LT, Perrino C (2020) Integrated evaluation of indoor particulate exposure: the VIEPI project. Sustainability 12(22):9758
41. American Society of Heating, Refrigerating and Air-Conditioning Engineers ASHRAE (2001) ASHRAE Handbook: Fundamentals, SI ed (ASHRAE Atlanta, GA., Atlanta, GA., 2001)
42. Shi Z, Lu Z, Chen Q (2019) Indoor airflow and contaminant transport in a room with coupled displacement ventilation and passive-chilled-beam systems. Build Environ 161:106244
43. Karam J, Ghali K, Ghaddar N (2023) Pulsating jet ventilation add-ons performance for reducing the contaminant spread in classrooms: Portable air cleaners vs. upper room UVGI. Build Environ 229:109946
44. Sørensen DN, Voigt LK (2003) Modelling flow and heat transfer around a seated human body by computational fluid dynamics. Build Environ 38(6):753–762
45. Gao N, Niu J (2004) CFD study on micro-environment around human body and personalized ventilation. Build Environ 39(7):795–805
46. Shan W, Rim D (2018) Thermal and ventilation performance of combined passive chilled beam and displacement ventilation systems. Energy and Buildings 158:466–475
47. Pei G, Rim D (2021) Quality control of computational fluid dynamics (CFD) model of ozone reaction with human surface: Effects of mesh size and turbulence model. Build Environ 189:107513
48. Chen Q (1995) Comparison of different $k-\varepsilon$ models for indoor air flow computations. Numer Heat Transf Part B: Fundam 28(3):353–369
49. Durrani F, Cook MJ, McGuirk JJ (2015) Evaluation of LES and RANS CFD modelling of multiple steady states in natural ventilation. Build Environ 92:167–181
50. Hu J, Kang Y, Lu Y, Yu J, Li H, Zhong K (2022) Numerical investigation of the thermal and ventilation performance of a combined impinging jet ventilation and passive chilled beam system. Build Environ 226:109726
51. Latif H, Maccarini A, Hultmark G, Nielsen PV, Rahnama S, Afshari A (2023) The establishment of design criteria for precision ventilation in open-plan offices. Build Environ 238:110378
52. Van Hooff T, Blocken B (2013) CFD evaluation of natural ventilation of indoor environments by the concentration decay method: CO2 gas dispersion from a semi-enclosed stadium. Build Environ 61:1–17
53. Kays WM (1994) Turbulent prandtl number—where are we? J Heat Transfer 116(2):284–295
54. Weller HG, Tabor G, Jasak H, Fureby C (1998) A tensorial approach to computational continuum mechanics using object-oriented techniques. Comput Phys 12(6):620
55. Abanto J, Barrero D, Reggio M, Ozell B (2004) Airflow modelling in a computer room. Build Environ 39(12):1393–1402
56. Liu S, Wang Z, Schiavon S, He Y, Luo M, Zhang H, Arens E (2020) Predicted percentage dissatisfied with vertical temperature gradient. Energy Build 220:110085
57. Davidson L, Olsson E (1987) Calculation of age and local purging flow rate in rooms. Build Environ 22(2):111–127
58. Ren J, He J, Novoselac A (2023) Predicting indoor particle concentration in mechanically ventilated classrooms using neural networks: model development and generalization ability analysis. Build Environ 238:110404
59. Nielsen PV, Restivo A, Whitelaw JH (1978) The velocity characteristics of ventilated rooms. J Fluids Eng 100(3):291–298
60. P.V. Nielsen (1974) Flow in Air Conditioned Rooms, PhD Thesis, Technical University of Denmark

Authors and Affiliations

P. G. Ledda[1] · M. G. Badas[1] · P. Monti[2] · A. Pelliccioni[3] · G. Querzoli[1]

✉ G. Querzoli
querzoli@unica.it

1 DICAAR, Università degli Studi di Cagliari, Cagliari, Italy

2 DICEA, Sapienza Università di Roma, Rome, Italy

3 DIMEILA, Istituto Nazionale per l'Assicurazione contro gli Infortuni Sul Lavoro, Rome, Italy